# A Quasielastic Neutron Scattering Investigation on the Molecular Self-Dynamics of Human Myelin Protein P2

*Saara Laulumaa*[†,‡], *Michael Marek Koza*[§], *Tilo Seydel*[§], *Petri Kursula*[†,⊥,*] *and Francesca Natali*[§,∥,*]

[†]Faculty of Biochemistry and Molecular Medicine and Biocenter Oulu, University of Oulu, Finland. [‡]European Spallation Source, Lund, Sweden. [§]Institut Laue-Langevin, Grenoble, France. [⊥]Department of Biomedicine, University of Bergen, Norway. [∥]CNR-IOM, OGG, Grenoble, France.

**ABSTRACT.** The human myelin protein P2 is a membrane binding protein believed to maintain correct lipid composition and organization in peripheral nerve myelin. Its function is related to its ability to stack membranes, and this function can be enhanced by the P38G mutation, whereby the overall protein structure does not change, but the molecular dynamics increase. Mutations in P2 are linked to human peripheral neuropathy. Here, the dynamics of wild-type P2 and the P38G variant were studied using quasielastic neutron scattering on time scales from 10 ps to 1 ns at 300 K. The results suggest that the mutant protein dynamics are increased on both the fastest and the

slowest measured time scales, by increasing the dynamics amplitude and/or the portion of atoms participating in the movement.

## 1. INTRODUCTION

Myelin is a tightly packed isolating membrane multilayer surrounding the neuronal axons in central (CNS) and peripheral nervous systems (PNS). It enables undisturbed fast saltatory conduction of axonal nerve impulses and thus enables the interplay between nerve cells and target tissues with distances in the meter scale. PNS myelin, consisting of 75-80% lipids and a specific selection of myelin proteins, is enfolded around axons by Schwann cells.[1-3]

Myelin protein P2 is one of the most abundant proteins in human PNS myelin. It is not present ubiquitously in myelin, but is enriched in selected areas, comprising locally up to 15% of myelin proteins.[4,5] P2 is a fatty acid binding protein (FABP), it binds cholesterol, and can attach membrane vesicles together in solution.[6-8] P2 is thus supposed to participate in lipid homeostasis in myelin.[8] With respect to specific diseases, P2 has been connected to autoimmune neuropathies[9] and Charcot-Marie-Tooth disease (CMT)[10-13]. CMT is a hereditary peripheral neuropathy caused by mutations in dozens of genes, including that coding for P2. While the P2 CMT disease mutations have only small effects on the crystal structure, they destabilize the P2 protein and affect its membrane binding properties.[14] The disease variants are more dynamic than wild-type P2, and the β-barrel structure of P2 opens more easily, which might be of relevance for ligand entry and egress.[14,15]

Previously, we reported the atomic-resolution crystal structure of human P2, showing the internal water molecules and hydrogen bond networks at atomic resolution.[7] We investigated the dynamics of the wild-type P2 protein (wtP2) and its proline-38-to-glycine mutated form (P2-

P38G) using computer simulations and elastic incoherent neutron scattering (EINS), suggesting that the dynamics of selected parts of the protein play a key role in the protein-lipid interactions and thus in the biological function of P2.[7,16,17] Pro38 is located at a possible hinge between helix α2 and strand β2 (Fig. 1). In functional and stability experiments, P38G and another portal region mutant, F57A, behave similarly to the point-mutated CMT disease variants (I43N, T51P, and I52T).[14-16] The role of protein dynamics in P2 function might be crucial, as upon the P38G point mutation, the atomic structure of the protein does not change, but the lipid membrane-stacking capacity of the protein is enhanced.[7] We previously measured EINS at energy resolutions from 70 μeV to 0.9 μeV and concluded that the P38G mutation increases the overall dynamics of P2 protein, especially on short time scales.[7] P2 is a β-barrel, formed by 10 β-strands with four connecting loops and two lid-like α-helices on the top of the barrel, which binds a fatty acid inside and lipid bilayers on the outside (Fig. 1).[6,7,18] Through computer simulations, the loops facing the lid have been shown to be the most flexible part of the P2 protein. The P38G mutation increases the flexibility of this portal region, which would then contribute to easier fatty acid egress and entry by P2.[15,16]

Here, we continue the P2 dynamics analyses through quasielastic neutron scattering (QENS) of hydrated wtP2 and P2-P38G protein powder samples to analyse the dynamics in detail. The QENS technique, like EINS, provides information on proton dynamics averaged over all the nuclei present in the sample, weighted by the corresponding scattering cross section (particularly high for H) and the amount of a specific atom. From the QENS spectra, information about specific types of dynamics in the measured time frame can be extracted. Here we calculate the time-space scale of each type of dynamics and proportion of atoms participating the movement. The spectra measured at energy resolutions from 70 μeV to 0.9 μeV enable the investigation of proton

dynamics on time scales from 10 ps to 1 ns. Within this time scale, a wide range of different atomic fluctuations in a protein occurs, starting from local atomic displacements to the larger-amplitude jumps of amino acid side chains. Neutron scattering offers a unique way to understand the contours of complex dynamics in biology, from small peptides and proteins[19] to cells[20] and tissues[21].

## 2. MATERIALS AND METHODS

**2.1 Sample preparation.** wtP2 and P2-P38G were produced recombinantly, purified, and prepared as hydrated powder samples, as described previously.[7] Briefly, proteins were expressed in *Escherichia coli* Rosetta (DE3) cells and purified using Ni-ion affinity and size-exclusion chromatography. 100 mg of both proteins were purified for the experiments described here. Buffer traces were removed in three rounds of dialysis against pure water, and the proteins were lyophilized and rehydrated with $D_2O$ in a $N_2/D_2O$ atmosphere, to achieve a hydration level of $h = 0.3$, where $h = m_{D_2O}/m_{protein}$. The hydrated protein samples were sealed in flat aluminum sample holders.

**2.2 Neutron scattering experiments.** The QENS spectra were collected on three instruments with different energy resolutions at the Institut Laue Langevin (ILL) in Grenoble: 70 μeV on IN6, 8 μeV on IN13, and 0.9 μeV on IN16.

IN6[22] is a time-of-flight spectrometer. Using a wavelength of 5.1 Å, the achieved 70 μeV energy resolution provides information on the 10 ps time scale dynamics. At this wavelength, the available $Q$ range is 0.4 Å$^{-1}$ < $Q$ < 2.0 Å$^{-1}$. IN13[23] is a backscattering spectrometer working with a wavelength of 2.23 Å and having an exceptionally high $Q$ range up to 4.9 Å$^{-1}$. IN13 has an energy resolution of 8 μeV, corresponding to ~100 ps time scale. The energy scans are performed by changing the

temperature of the $CaF_2$ monochromator crystals. Five scans in the range from -100 μeV to 100 μeV were carried out on the samples. The slowest dynamics in this experiment, on a ~1 ns time scale, were measured on IN16[24], which is a backscattering spectrometer with an energy resolution of 0.9 μeV. The instrument was working using a wavelength of 6.2 Å. Here, the energy change is achieved by moving the monochromator mounted on a Doppler drive. Data were acquired in the $Q$ range from 0.2 $Å^{-1}$ to 1.9 $Å^{-1}$.

All the QENS spectra were measured at 300 K, and the same samples were used on all three instruments. In order to avoid corrections from multiple scattering events, cell thickness was properly chosen to minimize neutron absorption by the sample. A typical transmission of ~95% was guaranteed using sample holders with thickness of 0.4-mm. The temperature is expected to be high enough to enable the necessary protein dynamics[25, 26], while low enough to avoid protein denaturation, as P2 protein starts to lose its secondary structure slightly above 320 K[16]. P2 protein samples do survive the harsh conditions of salt-free sample preparation and long experimental period of the set of our neutron scattering experiments, as the protein structure does not change during sample preparation and data collection.[16] 2 mm thick vanadium and empty cell spectra were used for data correction. LAMP[27] was used for data treatment, and spectral fitting was done using the model-independent software DAVE[28].

## 3. **THEORETICAL BASIS**

The IN6 spectra were fitted using one delta and one Lorentzian-shaped function for quasielastic broadening, both convoluted with the resolution function (Fig. 2). A flat background contribution was also included. To fit the IN13 spectra, the large Lorentzian component resolved on IN6 was added to the background, and the residual broadening was fitted using an additional Lorentzian

function. For IN16 data, the Lorentzian contribution resolved on IN13 was this time included to the fit together with a flat background, while a further narrow Lorentzian contribution was needed. According to Bee,[29] the calculated quasielastic scattering function $S(Q,\omega)$ can be approximated as

$$S(Q,\omega) = DWF \times S_{diff}(Q,\omega) \quad [1]$$

where DWF is the Debye-Waller factor of vibrational modes and $S_{diff}(Q,\omega)$ represents the diffusive contribution and can be written as

$$S_{diff}(Q,\omega) = A_0(Q) \times \delta(\omega) + \sum_{i=1}^{n} A_i \times L(Q_i,\omega), \quad [2]$$

with $A_0(Q)$ the elastic incoherent structure factor (EISF), and $L(Q,\omega)$ a standard Lorentzian function

$$L(Q,\omega) = \frac{1}{\pi}\frac{\Gamma(Q)}{\omega^2+\Gamma(Q)^2} \quad [3]$$

where $\Gamma(Q)$ defines its half-width at half-maximum.

**3.1 Jump diffusion.** In the jump diffusion model derived by Singwi and Sjölander[30], the hydrogen dynamics are described as combined oscillatory and diffusive motions. If the oscillatory period is much longer than the diffusion mean jump period ($\tau$), the width of the quasi-elastic peak is given by:

$$\Gamma(Q) = \frac{1}{\tau}\left[1 - \frac{e^{-2W}}{1+Q^2D\tau}\right] \quad [4]$$

with the Debye-Waller term 2W and a diffusion constant $D$. If the Debye-Waller term is considered small, $\Gamma(Q)$ can be written as

$$\Gamma(Q) = \frac{DQ^2}{1+DQ^2\tau}, \quad [5]$$

Where

$$l^2 = 2D\tau \quad [6]$$

with $l$ the jump length between the two sites and the mean square jump length in three dimensions $\langle x^2 \rangle = 3l^2$. At $Q^2D\tau \gg 1$, Γ(Q) approaches its asymptotic value

$$\Gamma_\infty = \frac{1}{\tau}. \quad [7]$$

At $Q^2D\tau \ll 1$, the model of Singwi and Sjölander reduces to the continuous diffusion model $\Gamma(Q) = DQ^2$. For protein samples, it is typical that in fast time scale dynamics, Γ(Q) does not approach zero at low $Q$ but a constant $\Gamma_0$ value.[31, 32] This is a feature of dynamics confined into a restricted volume, as described by Volino and Dianoux.[33] For diffusion inside an impermeable sphere with radius $r$, Γ(Q) reduces at low $Q$ to

$$\Gamma_0 = 4.33 * \hbar D/r^2. \quad [8]$$

For confined jump diffusion dynamics[34], the EISF is defined as

$$EISF_0(Q)_{jd} = \left(1 - p_{jd}\right) + p_{jd}\frac{2[1-\cos(Qd)]}{(Qd)^2} \quad [9]$$

where $p$ is the fraction of the atoms participating in the described movements and $d$ the size of confinement. For diffusion inside a sphere, the EISF is thus

$$EISF_0(Q)_{ds} = (1 - p_{ds}) + p_{ds}\left[\frac{3j_1(Qr)}{Qr}\right]^2 \quad [10]$$

where $j_1$ is the first-order spherical Bessel function.

**3.2 Methyl group rotation.** Methyl group rotation is considered to occur as jumps, where the movement of the three methyl hydrogen atoms is always connected in time and space. This three-site jump motion results in a $Q$ -independent Γ,

$$\Gamma = \frac{3}{2}\frac{\hbar}{\tau} \quad [11]$$

where $\tau$ is the average jump period.[29, 35]

The EISF of methyl group rotation can be written as

$$EISF(Q)_{met} = 1 - p_{met} + \frac{p_{met}}{3}\left[1 + 2j_0\left(Qr\sqrt{3}\right)\right] \quad [12]$$

where $j_0$ is a spherical Bessel function and $p_{met}$ the proportion of H belonging to the methyl groups. The radius $r$ (fixed to 1.03 Å) is calculated with an average methyl group C-H bond length of 1.09 Å and a bond angle of 109.5°.

If the EISF contains several different dynamical components, the fit can be presented as

$$EISF(Q) = (1 - p_1 - p_2) + p_1 EISF_1 + p_2 EISF_2 \quad [13]$$

where $EISF_1$ and $EISF_2$ can represent methyl group rotation, confined jump diffusion, or confined diffusion in a sphere.[36, 37]

## 4. RESULTS AND DISCUSSION

**4.1 Short-range protein dynamics.** The local, short-range atomic displacements in the protein were investigated on IN6, which provides access to fast (~10 ps) dynamics. The data were analyzed using a model, where proton dynamics is described by both jump diffusion and diffusion in a sphere.[34] In this model, the half-width of half-maximum (Γ(Q)) of the Lorentzian peak of quasielastic increases as a function of momentum transfer Q, showing different plateaus at both

low- and high-Q regions. Using Eq. 5 and 6, the average jump distances ($l$) and mean jump period ($\tau$) can be determined from the Γ dependence. In this case, the jump diffusion model presented by Singwi and Sjölander [30] (Eq. 5) is valid at higher Q values (Q > 0.5 Å$^{-1}$), where the Γ increases, facing a plateau related to the mean jump period in the high-Q region (Fig. 3). This model has been used also before for analyzing dynamics of hydrated protein powders from data collected on IN6.[31, 32, 35]

In the low-Q region, the Γ(Q) reaches a plateau $\Gamma_0$ (Eq. 8), which is related to the dynamics of atoms diffusing in a confined sphere, as described by Volino's model[33, 34] (Fig. 3). From the fit of the jump diffusion model (Eq. 5, 6), the resulting jump distances $l$ are around 1.5 Å for both wtP2 and P2-P38G (Table 1). Such a distance does not correspond to any hydrogen-hydrogen distances occurring in a protein, so the fit result represents an average of the localized motions and longer jumps seen the applied energy resolution window. The time scale of jump diffusion can be determined from the curvature of Γ(Q). The mean jump time $\tau$ is 4.8 ps for wtP2 and shorter, 3.7 ps, for P2-P38G (Table 1). The diffusion coefficient $D$ for jump diffusing atoms is similar for both wtP2 and P2-P38G, 2.7x10$^{-5}$ cm$^2$/s and 2.4x10$^{-5}$ cm$^2$/s respectively. To fit the EISF, both the jump diffusion model (Eq. 9) and diffusion in a sphere (Eq. 10) were used in combination (Eq. 13, Fig. 4, top), as has been done before[36, 37], to be coherent with the Γ(Q) fit, where the low-Q data were seen to face the low-Q plateau $\Gamma_0$ typical for the dynamics of diffusion in confinement. Pure diffusion within a sphere represents large-amplitude dynamics, and the EISF decays rapidly up to $Q^2 = 0.5$ Å$^{-2}$ (Fig. 4, bottom). At this low-Q region, the EISF of the jump diffusing atoms is small and covered by the wider Lorentzian peak of diffusion in a sphere contribution. Obviously, the larger-amplitude movement seen at low Q does not necessarily concern the same hydrogen group that participates in the jump diffusion movement. Thus, separated population fractions $p_1$ and $p_2$

are included in the EISF fit (Eq. 13). The fit with two EISF contributions (Fig. 4, bottom) is in good agreement with the Γ fit (Fig. 3), where the large-amplitude motion dominates at low $Q$ and jump-diffusion at higher Q-value. The EISF of jump diffusion describes the confined jump diffusion with $d$ as the size of confinement [34] being around 1.9 Å for both the wtP2 and P2-P38G (Table 1). In P2-P38G, 20% of the atoms participate in jump diffusion movement, whereas in wtP2, this fraction is much smaller, 14%. The diffusion in a confined sphere affects only a small portion of atoms, 5.7% of wtP2 and 8.0% of P2-P38G hydrogen atoms. The diffusion radius $R$ , ~ 6 Å for both samples, was extracted from EISF data. It was used to calculate the diffusion constant $D'$ for the large-amplitude movement (Eq.8). At low $Q$, the Γ settles to $\Gamma_0$ = 0.06 meV for wtP2 and to $\Gamma_0$ = 0.05 meV for P2-P38G resulting in $D'$ of $5.8 \times 10^{-5}$ cm²/s and $6.1 \times 10^{-5}$ cm²/s for wtP2 and P2-P38G, respectively. The non-restricted methyl groups have jump periods of a few picoseconds.[35] Earlier, Trapp *et al*. measured QENS for hydrated protein powders using the same instrument at 50 μeV and 70 μeV resolutions and determined resolution-dependent jump lengths of 1.8 and 0.7 Å, respectively.[32] The jump lengths determined here for P2 protein are consistent with those values. Together, the above results indicate that the dynamics observed on IN6 are instrument resolution-dependent, and that at a narrower resolution, more of the slower and longer-distance movements become detectable. The P38G mutation increases the overall dynamics of P2 protein on the picosecond time scale. The average jump time increases, and at the same time, the number of dynamic atoms increases significantly. This indicates that the point mutation enables slower dynamic contribution that slows down the average dynamics detected in the IN6 resolution window.

**4.2 Methyl group rotation.** The combination of an energy-accessible time scale (~100 ps) and a unique large Q-range (up to 4.9 $Å^{-1}$) makes IN13 an optimal instrument for observing methyl

group rotation.[23, 38] The main drawback of IN13 is the low neutron flux, which makes QENS data noisy and fitting challenging. To improve data quality, the data were binned over $Q$ in steps of $\Delta Q$ = 0.5 Å$^{-1}$. Γ(Q) data were fitted with one Lorentzian function representing methyl group rotation, which dominates the dynamics on the accessible time scale (Fig. 2). Moreover, as mentioned earlier, the large Lorentzian contribution determined from the fitting of IN6 data was here added to the background. The Γ(Q) of rotating methyl hydrogens, even if affected by large error bars, do not show here evident Q dependence; thus, it can be considered as constant Γ independent from the wavevector $Q$[29] (Eq. 11, Fig. 5). For both wtP2 and P2-P38G, Γ was estimated to be ~ 10 μeV, corresponding to a jump period $\tau$ = 90 ps (Fig. 5, Table 2). This value is in good agreement with simulation data presented by Roh *et al*.[39], where the average $\tau$ for dry lysozyme methyl groups was 110 ps and for wet lysozyme 75 ps at 295 K. Moreover, based on neutron scattering and NMR, the methyl group rotation period has been proposed to be highly dependent on the chemical environment of the hydrogens and vary from 10 to 200 ps, being fastest for methyl groups in methionine and slowest in alanine and threonine in computer simulations.[39-41] The EISF were fitted using the default methyl rotation radius $r$ = 1.03 Å, and thus, the hydrogen-hydrogen distance and jump length $d$ = 1.78 Å (Fig. 6). The fraction of atoms participating in this movement was estimated from the fit to be 0.25 ± 0.03 for wtP2 and 0.28 ± 0.03 for P2-P38G (Table 2). No statistically significant difference is seen between these fitting results. Both values are very close to the calculated methyl hydrogen fraction of 0.26 in P2.

**4.3 Large-amplitude dynamics.** In the 1 ns time window, all the methyl groups can be assumed to be rotating, as was shown by both NMR experiments[40, 42] as well as neutron scattering from dry and hydrated lysozyme[39]. Thereby IN16 can be used for observing the rearrangement of amino acid side chains. The broadening of the elastic peak measured on IN16 could be fitted using only

two Lorentzian functions (Fig. 2). The fitting suggests that only two main dynamical features are predominant: the fast methyl group rotation and the slower jump diffusion of side chains fluctuating between different conformations. It should be underlined that on the slow 1 ns time scale, a huge variety of different movements occurs, and the used model describes the nature of the average dynamics in the observed time scale.

The Γ behavior of the methyl group rotation contribution was fixed based on the fit to IN13 data, while the fitting parameters for the slower component were set free. As data collected on IN13 are rather noisy, making the determination of the Γ behaviour of the methyl group component challenging, boundary limits were initially given to the fit of Γ of methyl rotation, centered at the starting fitting value Γ = 10 μeV. A check of the fitting sensibility for Γ revealed that changing Γ slightly does not drastically affect the fitting result for the slower component, and thereby the fixed values were used. The Γ(Q) of both wtP2 and P38G face a plateau around 1.5 μeV, corresponding to a mean jump period τ of ~400 ps (Fig. 7, Table 3). The calculated *D* of the jump diffusion (Eq. 6) is ~0.3 x $10^{-5}$ $cm^2/s$ for wtP2 and corresponding jump length *l* of ~5 Å. The Γ(Q) data quality of P2-P38G was not good enough to properly define *D* and *l* parameters. The EISF from the IN16 data were fitted combining methyl group rotation and confined jump diffusion functions (Eq. 9, 12, 13, Fig. 8). The fraction of methyl group hydrogens was fixed to the theoretical value of 0.26, assuming that all methyl groups rotate in the observed time scale of 1 ns[38]. The EISF of the methyl group component has a minimum above Q = 2.5 $Å^{-1}$ (Fig. 6), so it decreases slowly within the above-monitored Q-range up to Q = 2 $Å^{-1}$ (Fig. 8, bottom). The EISF of the larger-amplitude movements of the confined jump diffusion particles has a minimum around Q = 1 $Å^{-1}$ which corresponds to sizes of confinement *d* of 5.5 Å and 5.7 Å in wtP2 and P38G, respectively (Fig. 8, Table 3). The occupancy of this motion is ~0.24 for wtP2 and ~0.30, for P2-P38G (Table 3).

The described slow jump diffusion dynamics could be assigned to amino acid side chain conformational rearrangements. Indeed, up to 5 Å distances between side chain hydrogen atoms can be seen even in crystal structures at cryogenic temperatures, for example in alternative conformations of side chains Ile41 and Lys158 of P2, as shown in Fig. 9. The EISF fit indicates a higher flexibility of the mutated protein compared to wtP2 in nanosecond time scale. The result is coherent with the IN6 data and previously reported EINS experiments[16], in which the P38G mutation increased the protein flexibility, especially in slow time scale dynamics close to physiological temperatures.

## 5. CONCLUSIONS

The P38G mutation was previously shown to increase the overall dynamics of the P2 protein.[16] Here, in a more detailed dynamics study, we have shown that P2-P38G is more dynamic than wtP2 at all used energy resolutions from 10 ps to 1 ns time windows. Already in the fast 10 ps dynamics, measured on IN6, the contribution of atoms participating in local atom displacements is higher for P2-P38G than for P2wt. Slightly longer-range jumps are seen in the same time window, and thus, the jump length, and the mean jump period of P2-P38G are increased compared to wtP2. The methyl group contribution, seen on IN13, was very similar for wtP2 and P2-P38G proteins and possible small differences could not be detected with the current data quality. Differences in EISF, and thus, in the proportion of the fast time scale dynamics, could not be defined due to high background levels in the spectra. However, the fitted values for methyl group rotation were physiologically relevant and could be included into IN16 data fitting. IN16 results confirm the enhanced flexibility of P2-P38G compared to wtP2 on the 1 ns time scale. As at faster time scales, the proportion of atoms in P2-P38G facing the jump diffusion is higher, while the estimated jump length is similar for both the wtP2 and P2-P38G. P38G, which has a mutation in the hinge region

of the P2 helical lid, appears to increase the dynamics of P2 on many levels. Interestingly, in functional assays, P38G behaves very similarly to the CMT disease mutations recently discovered for human P2.[11-14, 16] An obvious future goal is to study the fine details of proteins carrying the CMT disease mutations, with respect to the dynamics of the protein and the lipid membrane it is associated with.

## AUTHOR INFORMATION

### Corresponding Authors

Petri Kursula, +47 55 58 64 38, petri.kursula@uib.no; Francesca Natali, +33 (0)4 76 20 70 71, natali@ill.fr.

### Author Contributions

Study design: S.L., P.K., F.N.; Protein expression and purification: S.L.; Sample preparation: S.L.; Data collection: F.N., S.L., M.M.K., T.S.;, Data analysis: S.L., F.N.; Supervision: P.K., F.N.; Funding: P.K., F.N.; Manuscript writing: S.L., M.M.K., T.S., P.K., F.N. All authors have given approval to the final version of the manuscript.

### Funding Sources

This work was financially supported by the European Spallation Source, the Academy of Finland, the Emil Aaltonen Foundation (Finland), and the Sigrid Jusélius Foundation (Finland).

## ACKNOWLEDGMENT

We would like to thank the Institute Laue Langevin for the beamtime on IN6, IN16, and IN13, as well as Miguel Gonzales (ILL) for his valuable help in data correction.

## ABBREVIATIONS

CMT, Charcot-Marie-Tooth disease; CNS, central nervous system; EINS, elastic incoherent neutron scattering; EISF, elastic incoherent structure factor; FABP, fatty acid binding protein; ILL, Institut Laue-Langevin; PDB, protein data bank; PNS, peripheral nervous system; P2-P38G, proline-38-to-glycine mutated P2 protein; QENS, quasielastic neutron scattering; wtP2, wild-type P2-protein.

## REFERENCES


(1) E. D. Buttermore; C. L. Thaxton; M. A. Bhat. Organization and maintenance of molecular domains in myelinated axons. *J. Neurosci. Res.* **2013**, 91(5), 603-22.

(2) H. Han; M. Myllykoski; S. Ruskamo; C. Wang; P. Kursula. Myelin-specific proteins: a structurally diverse group of membrane-interacting molecules. *BioFactors* **2013**, 39(3), 233–41.

(3) J. S. O'Brien; E. L. Sampson. Lipid composition of the normal human brain: gray matter, white matter, and myelin. *J. Lipid Res.* **1965**, 6(4), 537-44.

(4) S. Greenfield; S. Brostoff; E. H. Eylar; P. Morell. Protein composition of myelin of the peripheral nervous system. *J. Neurochem.* **1973**, 20(4), 1207–16.

(5) B. D. Trapp; L. J. McIntyre; R. H. Quarles; N. H. Sternberger; H. D. Webster. Immunocytochemical localization of rat peripheral nervous system myelin proteins: P2 protein is not a component of all peripheral nervous system myelin sheaths. *Proc. Natl. Acad. Sci. U. S. A.* **1979**, 76(7), 3552-6.

(6) T. A. Jones; T. Bergfors; J. Sedzik; T. Unge. The three-dimensional structure of P2 myelin protein. *EMBO J.* **1988**, 7(6), 1597-604.

(7) S. Ruskamo; R. P. Yadav; S. Sharma; M. Lehtimäki; S. Laulumaa; S. Aggarwal; M. Simons; J. Bürck; A. S. Ulrich; A. H. Juffer; et al., . Atomic resolution view into the structure-function relationships of the human myelin peripheral membrane protein P2. *Acta Cryst. D* **2014**, 70, 165-76.

(8) J. Zenker; M. Stettner; S. Ruskamo; E. Domènech-Estévez; H. Baloui; J. J. Médard; M. H. G. Verheijen; J. F. Brouwers; P. Kursula; B. C. Kieseier; et al. A role of peripheral myelin protein 2 in lipid homeostasis of myelinating Schwann cells. *Glia* **2014**, 62(9), 1502-1512.

(9) M. Offenhausser; A. S. Herr; J. Hartkamp; M. Wauben; T. Magnus; O. Grauer; S. Seubert; A. Weishaupt; K. V. Toyka; R. Gold; et al. Truncation of the neuritogenic peptide bP2(60-70) results in the generation of altered peptide ligands with the potential to interfere with T cell activation. *J. Neuroimmunol* **2002**, 129(1-2), 97-105.

(10) C. Gonzaga-Jauregui, T. Harel, T. Gambin, M. Kousi, L. B. Griffin, L. Francescatto, B. Ozes, E. Karaca, S. N. Jhangiani, M. N. Bainbridge, et al. Exome Sequence Analysis Suggests that Genetic Burden Contributes to Phenotypic Variability and Complex Neuropathy. *Cell Rep*. **2015**, 12(7), 1169-83.

(11) Y. B Hong; J. Joo; Y. S. Hyun; G. Kwak; Y. R. Choi; H. K. Yeo; D. H. Jwa; E. J. Kim; W. M. Mo; S. H. Nam; et al. A Mutation in PMP2 Causes Dominant Demyelinating Charcot-Marie-Tooth Neuropathy. *PLoS Genet*. **2016**, 12(2), e1005829.

(12) W. W. Motley; P. Palaima; S. W. Yum; M. A. Gonzalez; F. Tao; J. V. Wanschitz; A. V. Strickland; W. N. Löscher; E. Vriendt; S. Koppi; et al. De novo PMP2 mutations in families with type 1 Charcot-Marie-Tooth disease. *Brain* **2016**, 139, 1649–56.

(13) J. Punetha; L. Mackay-Loder; T. Harel; Z. Coban-Akdemir; S. N. Jhangiani; R. A. Gibbs; I. Lee; D. Terespolsky; J. R. Lupski; J. E. Poseya. Identification of a pathogenic PMP2 variant in

a multi-generational family with CMT type 1: Clinical gene panels versus genome-wide approaches to molecular diagnosis. *Mol. Genet. Metab.* **2018**, 125(3), 302-4.

(14) S. Ruskamo; T. Nieminen; C. K. Kristiansen; G. H. Vatne; A. Baumann; E. I. Hallin; A. Raasakka; P. Joensuu; U. Bergmann; I. Vattulainen; et al. Molecular mechanisms of Charcot-Marie-Tooth neuropathy linked to mutations in human myelin protein P2. *Sci. Rep.* **2017**, 7(1), 6510.

(15) S. Laulumaa; T. Nieminen; A. Raasakka; O.C. Krokengen; A. Safaryan; E.I. Hallin; G. Brysbaert; M.F. Lensink; S. Ruskamo; I. Vattulainen; et al. Structure and dynamics of a human myelin protein P2 portal region mutant indicate opening of the β barrel in fatty acid binding proteins. *BMC Struc. Biol.* **2018**, 18(1), 8.

(16) S. Laulumaa; T. Nieminen; M. Lehtimäki; S. Aggarwal; M. Simons; M. M. Koza; I. Vattulainen; P. Kursula; F. Natali. Dynamics of the Peripheral Membrane Protein P2 from Human Myelin Measured by Neutron Scattering--A Comparison between Wild-Type Protein and a Hinge Mutant. *PLoS One* **2015**, 10(6), e0128954.

(17) S. Laulumaa; P. Kursula; F. Natali. Neutron scattering studies on protein dynamics using the human myelin peripheral membrane protein. *P2 EPJ Web Conf.* **2015**, 83, 02010.

(18) V. Majava; E. Polverini; A. Mazzini; R. Nanekar; W. Knoll; J. Peters; F. Natali; P. Baumgärtel; I. Kursula; P. Kursula. Structural and functional characterization of human peripheral nervous system myelin protein P2. *PLoS ONE* **2010**, 5(4), e10300.

(19) G. Schiró; C. Caronna; F. Natali; A. Cupane. Direct Evidence of the Amino Acid Side Chain and Backbone Contributions to Protein Anharmonicity. *J. Am. Chem. Soc.* **2010**, 132, 1371-6.

(20) A. M. Stadler; J.P. Embs; I. Digel; G. M. Artmann; T. Unruh. Cytoplasmic water and hydration layer dynamics in Human red blood cells. *J. Am. Chem. Soc.* **2008**, 130, 16852-3.

(21) F. Natali, C. Dolce, J. Peters, C. Stelletta, B. Deme, J. Ollivier, M. Boehm, G. Leduc, I. Piazza, A. Cupane, et al. Anomalous water dynamics in brain: a combined diffusion Magnetic Resonance Imaging and Neutron Scattering investigation. *J. Royal Soc. Interface.* In press.

(22) Y. Blanc. Le Spectrometre A Temps De Vol IN6, characteristiques, techniques at performances. *ILL report* **2010** 83Bl21G.

(23) F. Natali; J. Peters; D. Russo; S. Barbieri; C. Chiapponi; A. Cupane; A. Deriu; M.T. Di Bari; E. Farhi; Y. Gerelli; et al. IN13 Backscattering Spectrometer at ILL: Looking for Motions in Biological Macromolecules and Organisms. *Neutron News*, **2008**, 19, 14-8.

(24) B. Frick; M. Gonzalez. Five years operation of the second generation backscattering spectrometer IN16—a retrospective, recent developments and plans. *Phys. B: Cond. Matt.* **2001**, 301(1-2), 8-19.

(25) W. Doster. The two-step scenario of the protein dynamical transition. *J. Non-Crys. Sol.* **2011**, 357, 622-628.

(26) G. Schiro; F. Natali; A. Cupane. Physical origin of anharmonic dynamics in proteins: new insights from resolution-dependent neutron scattering on homomeric polypeptides. *Phys. Rev. Lett.* **2012**, 109(12), 128102.

(27) D. Richard; M. Ferrand; G. J. Kearley. Analysis and visualisation of neutron-scattering data *J. Neutron Res.* **1996**, 4(1-4), 33-9.

(28) R. T. Azuah; L. R. Kneller; Y. Qiu; P. L. W. Tregenna-Piggott; C. M. Brown; J. R. D. Copley; R.M. Dimeo. DAVE: A Comprehensive Software Suite for the Reduction, Visualization,

and Analysis of Low Energy Neutron Spectroscopic Data. *J. Res. Natl. Inst. Stan. Technol.* **2009**, 114(6), 341-58.

(29) M. Bée. *Quasielastic neutron scattering,* Adam Hilger, **1988**.

(30) K. S. Singwi; A. Sjolander. Diffusive Motions in Water and Cold Neutron Scattering *Phys. Rev.* **1960**, 119, 863.

(31) A. M. Stadler; C. J. Garvey; J. P. Embs; M. M. Koza; T. Unruh; G. Artmann; G. Zaccai. Picosecond dynamics in haemoglobin from different species: a quasielastic neutron scattering study. *Bioch. et Biophys. Acta* **2014**, 1840(10), 2989-99.

(32) M. Trapp; M. Tehei; M. Trovaslet; F. Nachon; N. Martinez; M. M. Koza; M. Weik; P. Masson; J. Peters. Correlation of the dynamics of native human acetylcholinesterase and its inhibited huperzine A counterpart from sub-picoseconds to nanoseconds. *J. R. Soc. Int.* **2014**, 11(97), 20140372.

(33) F. Volino; A. J. Dianoux. Neutron incoherent scattering law for diffusion in a potential of spherical symmetry: general formalism and application to diffusion inside a sphere. *Mol. Phys.* **1980**, 41(2), 271-9.

(34) P. L. Hall; D. K. Ross. Incoherent neutron scattering functions for random jump diffusion in bounded and infinite media. *Mol. Phys.* **1981**, 42(3), 673.-82.

(35) J. Fitter; R. E. Lechner; G. Buldt; N. A. Dencher. Internal molecular motions of bacteriorhodopsin: hydration-induced flexibility studied by quasielastic incoherent neutron scattering using oriented purple membranes. *Proc. Natl. Acad. Sci. U. S. A.* **1996**, 93(15), 7600-5.

(36) S. Fujiwara; M. Plazanet; F. Matsumoto. Internal motions of actin characterized by quasielastic neutron scattering. *T. Oda, Eur. Biophys. J.* **2011**, 40(5), 661-71.

(37) J. D. Nickels, V. Garcia-Sakai and A. P. Sokolov. Dynamics in protein powders on the nanosecond-picosecond time scale are dominated by localized motions. *J. Phys. Chem. B* **2013**, 117(39), 11548-55.

(38) J. H. Roh; V. N. Novikov; R. B. Gregory; J. E. Curtis; Z. Chowdhuri; A. P. Sokolov. Onsets of anharmonicity in protein dynamics. *Phys. Rev. Lett.* **2005**, 95(3), 038101.

(39) J. H. Roh; J. E. Curtis; S. Azzam; V. N. Novikov; I. Peral; Z. Chowdhuri; R. B. Gregory; A. P. Sokolov. Influence of hydration on the dynamics of lysozyme. *Biophys. J.* **2006**, 91(7), 2573-88.

(40) R. B. Best; J. Clarke; M. Karplus. What contributions to protein side-chain dynamics are probed by NMR experiments? A molecular dynamics simulation analysis. *J. Mol. Biol.* **2005**, 349(1), 185-203.

(41) M. Tehei; J. D. Perlmutter; F. Giusti; J. N. Sachs; G. Zaccai; J. L. Popot. Thermal fluctuations in amphipol A8-35 particles: a neutron scattering and molecular dynamics study. *J. Membr. Biol.* **2014**, 247(9-10), 897-908.

(42) W. Liu; E. Crocker; D. J. Siminovitch; S. O. Smith. Role of side-chain conformational entropy in transmembrane helix dimerization of glycophorin A. *Bioph. J.* **2003**, 84(2), 1263-71.

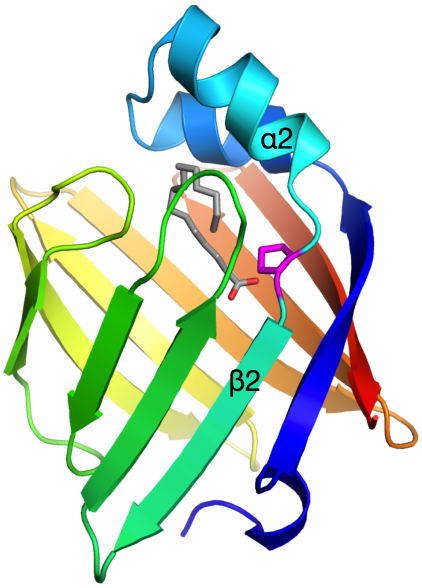


**Figure 1.** Cartoon representation of the wtP2 crystal structure (PDB code: 4BVM). Bound palmitate, carried over from *E. coli*, is shown in gray and Pro38 in magenta.

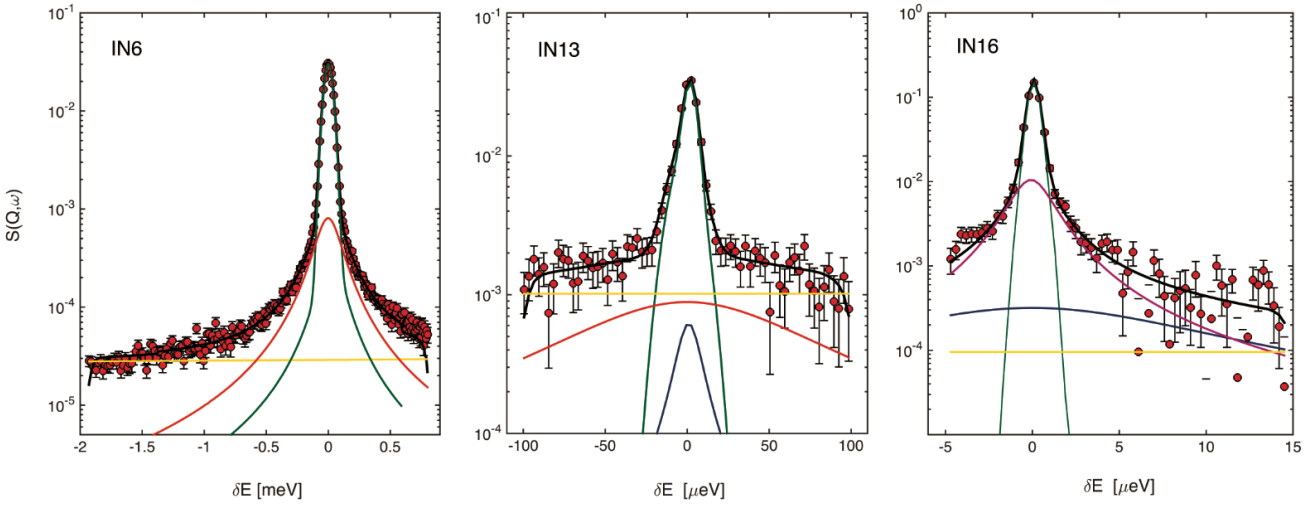


**Figure 2.** Fits to quasielastic spectra of wtP2 measured on IN6, IN13 and IN16 at Q = 1.0 Å$^{-1}$. The black line represents the total fit as the convolution of the resolution function with a delta function (green) and a set of Lorentzian functions representing fast jump diffusion (red), methyl rotation (blue) and slow jump diffusion (magenta). A flat background (yellow) is also included. The spectra are truncated in the plots to highlight the region of interest.

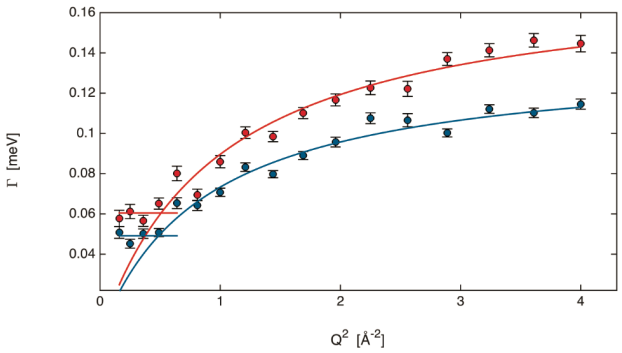


**Figure 1.** Γ parameters derived from IN6 data using the jump diffusion model ($0.5 < Q^2 < 4$) and the model of diffusion inside a sphere ($0.2 < Q^2 < 0.7$). wtP2 is shown in red and P2-P38G in blue.

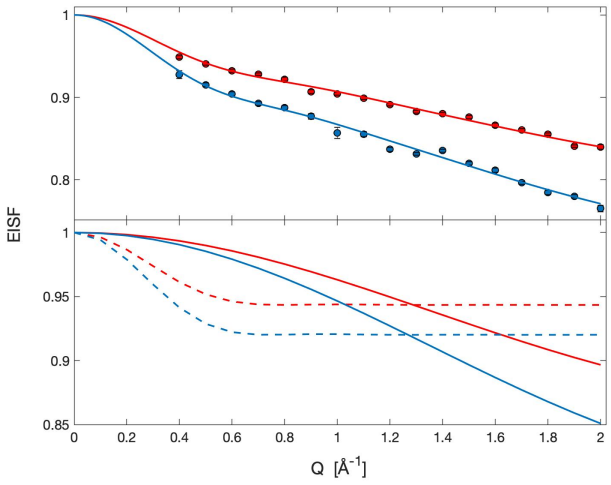


**Figure 2.** Top: Fitting EISF of IN6 data using the jump diffusion model with jump length of 1.5 Å and diffusion in a sphere model. Bottom: EISF contributions of diffusion in a sphere (dashed line) and jump diffusion (solid line). Red: wtP2; blue: P2-P38G.

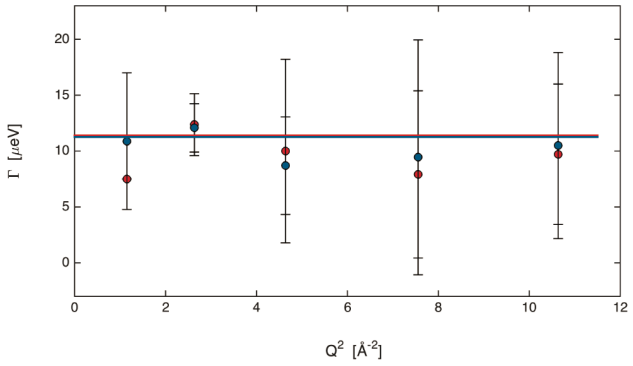


**Figure 3.** IN13 Γ and data fit using the three-site jump model. wtP2 is shown in red, P2-P38G in blue.

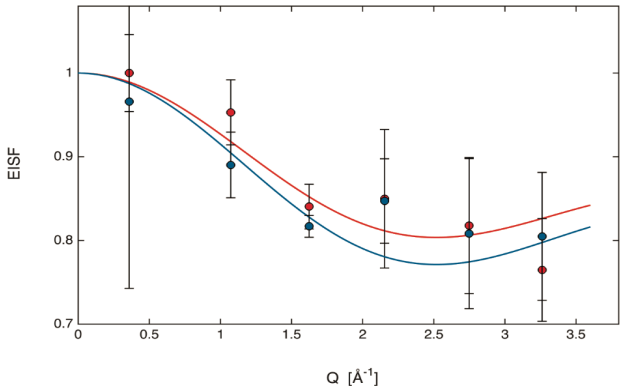


**Figure 4.** Fitting the EISF from IN13 data using the methyl group rotation model. wtP2 is shown in red, P2-P38G in blue.

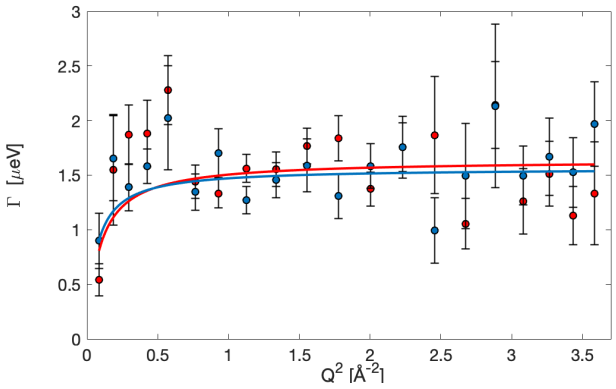


**Figure 7.** Γ from IN16 data and fit to the jump diffusion model (wtP2 data in red, P2-P38G in blue).

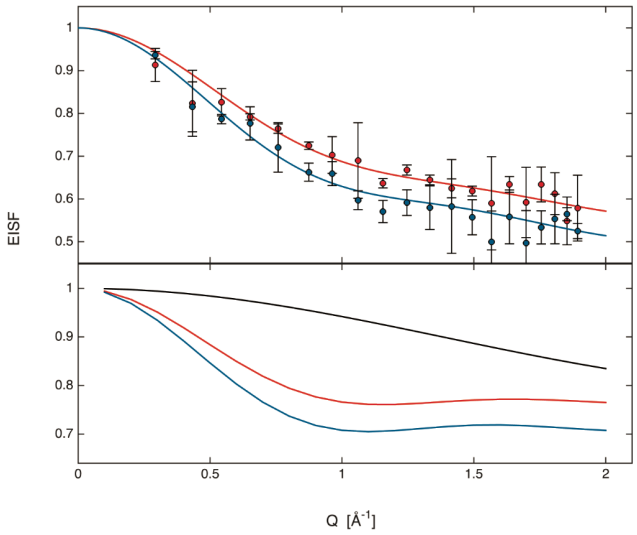


**Figure 8.** Top: IN16 EISF fitted using a combination of methyl rotation and jump diffusion models, wtP2 in red and P2-P38G in blue. Bottom: Methyl group rotation (fixed to p = 0.26) shown with black line, jump diffusion contributions shown with red line for wtP2 and blue line for P2-P38G.

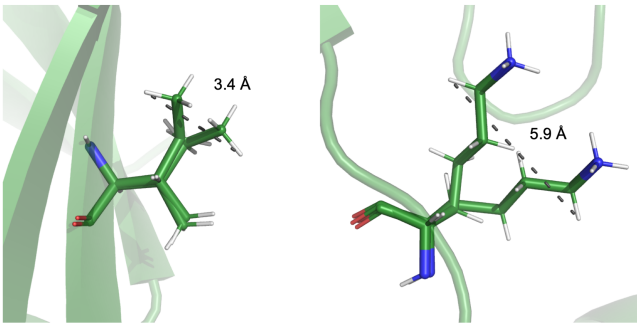


**Figure 9.** Ile41 (left) and Lys158 (right) have two alternative conformations in the wtP2 crystal structure (PDB code: 4BVM). The longest distances between hydrogens in two conformations are shown with dashed lines. The structure was determined at 100 K.

| Jump diffusion | *wtP2* | *P2-P38G* |
|---|---|---|
| $D$ [$10^{-5}$ cm$^2$/s] | 2.7 ± 0.3 | 2.4 ± 0.2 |
| $\tau$ [ps] | 3.7 ± 0.2 | 4.8 ± 0.2 |
| $l$ [Å] | 1.4 ± 0.2 | 1.5 ± 0.2 |
| $d$[Å] | 1.9 ± 0.3 | 1.9 ± 0.3 |
| $p_1$ | 0.14 ± 0.02 | 0.20 ± 0.03 |
| Diffusion inside a sphere | *wtP2* | *P2-P38G* |
| $D$' [$10^{-5}$ cm$^2$/s] | 7.1 ± 0.4 | 6.4 ± 0.3 |
| $R$ [Å] | 5.8 ±0.7 | 6.1 ± 0.9 |
| $p_2$ | 0.057 ± 0.005 | 0.080 ± 0.008 |

**Table 1.** Parameters derived from IN6 and EISF data using the models of jump diffusion and diffusion inside a sphere.

| Rotation of methyl groups | *wtP2* | *P2-P38G* |
|---|---|---|
| $\tau$ [ps] | 90 ± 10 | 88 ± 7 |
| *p* | 0.25 ± 0.03 | 0.28 ± 0.02 |

**Table 2.** IN13 data fitting parameters for the methyl group rotation fit.

| Jump diffusion | wtP2 | P2-P38G |
|---|---|---|
| *p* | 0.239 ± 0.004 | 0.295 ± 0.008 |
| *l* [Å] | 5 ± 3 | * |
| *d* [Å] | 5.5 ± 0.2 | 5.7 ± 0.2 |
| $\tau$ [ps] | 400 ± 20 | 420 ± 10 |
| *D* [$10^{-5}$ $cm^2/s$] | 0.3 ± 0.2 | * |

**Table 3.** Fitting parameters for IN16 EISF and Γ, of a Lorentzian function representing large amplitude jump diffusion dynamics.

The theoretical values p = 0.26 and r = 1.03 Å were fixed for the methyl group contribution.
* Values could not be determined due to poor statistics.